ACES Asian Chemical Editorial Society

DOI: 10.1002/asia.201701741

CHEMISTRY AN ASIAN JOURNAL Full Paper

Calixarenes

Transformations in Chemically Responsive Copper-Calixarene Architectures

Edmundo G. Percástegui,*[a, d] Carlos Reyes-Mata,[a] Marcos Flores-Alamo,[b] Beatriz Quiroz-García,[a] Ernesto Rivera,[c] and Ivan Castillo*[a]

Abstract: Self-assembly of bis-picolyl-appended calix[4]arene (**L**) with Cu^{I} or Cu^{II} salts resulted in a collection of multinuclear architectures capable of expressing structural reconfigurations in response to various chemical stimuli: addition of copper salt, solvents, or oxidation. Coordination of **L** to CuX (X = Br, I) selectively yielded dinuclear macrocycles $\mathbf{Cu^{I}_2L_2Br_2}$ (**1**) and $\mathbf{Cu^{I}_2L_2I_2}$ (**3**) that were transformed into tetranuclear assemblies $\mathbf{Cu^{I}_4L_2Br_4}$ (**2**) and $\mathbf{Cu^{I}_4L_2I_4}$ (**4**) upon further addition of CuX. These supramolecules persist as robust and discrete entities in solution that display red emission; notably, **4** exhibits luminescence thermochromism. Assembly of **L** with $CuCl_2$ produced macrocycle $\mathbf{Cu^{II}_2L_2Cl_4}$ (**5**), which crystallised as cage $\mathbf{[Cu^{II}_2L_4(\mu\text{-}Cl)]^{3+}}$ (**6**) in the presence of MeOH. Two chemical signals—introduction of $CuCl_2$ and addition of CH_3CN—regenerated macrocycle **5**. Coordination of **L** to Cu(OTf) yielded macrocycle $\mathbf{Cu^{I}_2L_2(OTf)_2}$ (**7**) that also crystallised as cage **6** upon oxidation in $CHCl_3$.

Introduction

Natural systems express structural adaptations and functions upon receipt of precise chemical instructions. Inspired by nature, supramolecular abiological entities that are likewise able to respond to chemical stimuli have been created as the basis to decipher the fundamentals of responsive chemical networks in life, and to enable the design of programmable dynamic architectures and materials.[1]

In recent years, metal-directed self-assembly has proven useful for constructing stimuli-responsive supramolecules of increasing complexity and intricate functionality by virtue of the reversible nature of metal-donor associations.[1,2] To date, most available systems contain Fe^{II}, Co^{II}, Zn^{II}, Pd^{II} and Cd^{II} ions as dynamic functions that allow structural reconfigurations in response to sequences of external chemical inputs such as metals, components, solvents, anions, or guests.[2,3] Although the engineering of stimuli-responsive systems has seen tremendous progress in recent years, the precise induction of transformations to achieve fine-tuning of targeted properties remains challenging, and it requires improving structural diversity as well as a higher understanding on how to control responsiveness.

Herein, we present a family of macrocyclic structures, obtained via self-assembly of bis(4-picolyl)-*p*-tert-butylcalix[4]arene (**L**) with Cu^{I} or Cu^{II} halides, these structures feature structural adaptations in response to different chemical signals (Figure 1). Previously, we informed that assembly of **L** with Zn^{II}, Pd^{II}, Ag^{I}, and Cd^{II} led to formation of blue-emissive [2+2] metallacycles in all cases, despite the varied metal identity.[4] Unlike the former systems, the supramolecules herein presented evidence that copper ions are not only spectator structural motifs, but they can also introduce chemical responsiveness and cause dramatic alterations on supramolecular organisation and emissive properties. While assembly with Cu^{I} selectively yielded red emissive dinuclear macrocycles that can convert into tetranuclear derivatives, coordination to Cu^{II} resulted in formation of a non-emissive dinuclear metallacycle that reversibly undergoes an unusual reconfiguration into a more intricate cage structure. Despite the promising optical, redox, and coordinative-labile attributes of $Cu^{I/II}$ ions, which may be advantageous for supramolecular catalysis, luminescence, or enzyme mimics,[5] their use as design element to construct adaptive supramolecular systems remains scarce.

[a] Dr. E. G. Percástegui, C. Reyes-Mata, Dr. B. Quiroz-García, Prof. I. Castillo
Instituto de Química
Universidad Nacional Autónoma de México, UNAM
Circuito Exterior, Ciudad Universitaria, 04510 (México)
E-mail: eg490@cam.ac.uk
joseivan@unam.mx

[b] Dr. M. Flores-Alamo
Facultad de Química
Universidad Nacional Autónoma de México, UNAM
Circuito Exterior, Ciudad Universitaria, 04510 (México)

[c] Prof. E. Rivera
Instituto de Investigaciones en Materiales
Universidad Nacional Autónoma de México, UNAM
Circuito Exterior, Ciudad Universitaria, 04510 (México)

[d] Dr. E. G. Percástegui
Current address:
Department of Chemistry
University of Cambridge
Lensfield Road, Cambridge, CB2 1EW (UK)

Supporting information and the ORCID identification number(s) for the author(s) of this article can be found under https://doi.org/10.1002/asia.201701741.

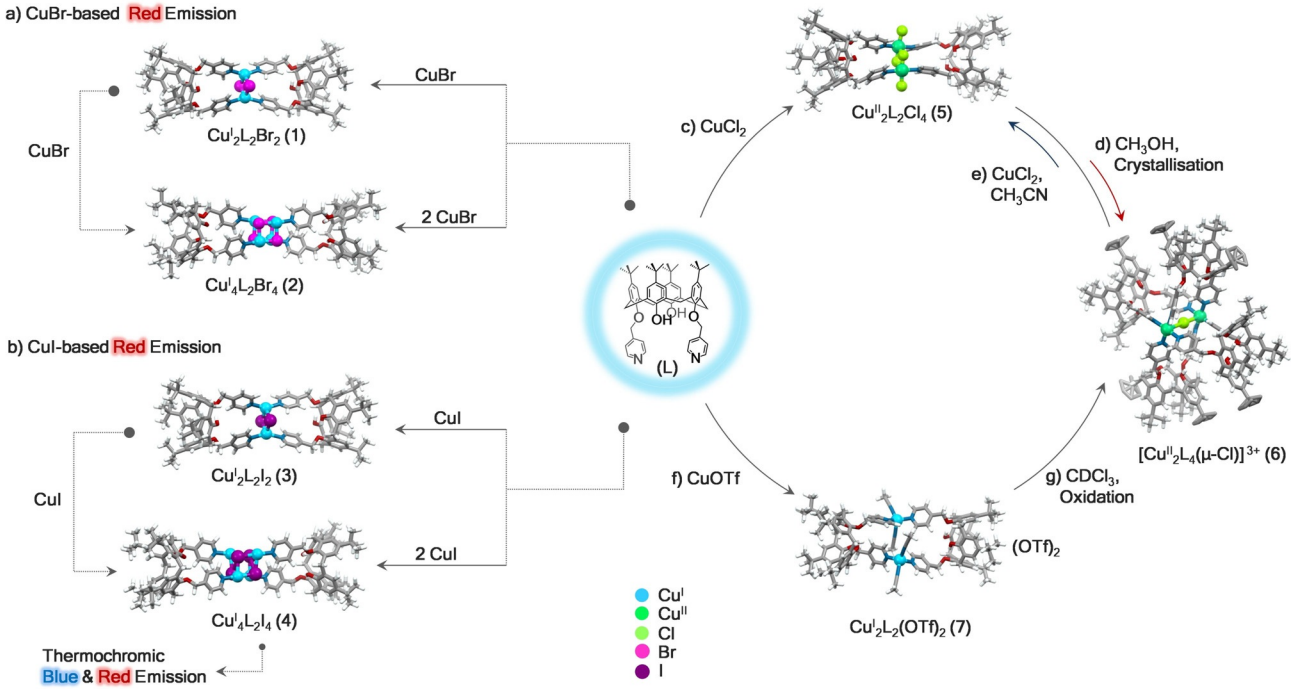

Figure 1. Self-assembly reactions and stimuli-responsive transformations of copper assemblies **1**–**7**. Mercury view of crystal structure of windmill-cage **6** (disordered atoms and solvents are omitted for clarity) along with perspective of MM3 minimised structures for **1**–**5** and **7**. a) Addition of 1 equiv. of CuBr to **L** produces **1**, which responds to further addition of CuBr to generate tetranuclear macrocycle **2**; direct assembly of **L** and 2 equiv. of CuBr also affords **2**. b) Reaction of **L** and 1 equiv. of CuI generates dinuclear structure **3**. Tetranuclear assembly **4** can be obtained either by further addition of CuI to **3** or by direct assembly of **L** and 2 equiv. of CuI. c) Equimolar reaction of **L** and $CuCl_2$ yields metallacycle **5**. d) Macrocycle **5** crystallises as windmill-cage **6** in the presence of CH_3OH. e) Addition of $CuCl_2$ to cage **6** in CH_3CN regenerates macrocycle **5**. f) Combination of equimolar amounts of **L** and CuOTf produces the metastable dinuclear copper-triflate complex **7**. g) Oxidation of **7** in $CDCl_3$ produces crystals of **6**.

Results and Discussion

Self-assembly of luminescent $Cu^{I}_nL_2X_n$ (X = Br, I; n = 2, 4) metallacycles 1–4

Initially, calixarene **L** was mixed with CuBr or CuI in equimolar ratios in CH_3CN affording as only products the corresponding dinuclear metallacycles $\mathbf{Cu_2L_2X_2}$ [X = Br (**1**) and I (**3**)] as microcrystalline precipitates that are soluble in $CHCl_3$ and CH_2Cl_2 but insoluble in polar solvents like CH_3CN or CH_3OH. Subsequently, these macrocycles were converted into the tetranuclear assemblies $\mathbf{Cu_4L_2Br_4}$ (**2**) and $\mathbf{Cu_4L_2I_4}$ (**4**) when suspended in CH_3CN and mixed with additional CuX (1.5 equiv) through simple Cu^{I}-induced transformations. Tetranuclear assemblies **2** and **4** could also be obtained by direct self-assembly of **L** and 2.2 equivalents of CuX in CH_3CN as microcrystals soluble in chlorinated solvents but not in polar organic solvents (Figures 1 a and 1 b). Further addition of CuX to tetranuclear species **2** and **4** did not alter their stoichiometry; hence, assemblies of higher order were not observed, thus indicating that nuclearity is limited by the aperture of picolyl coordinating vectors.

The ^{1}H NMR spectra of assemblies **1**–**4** display one set of resonances that corresponds to a single calixarene environment and is consistent with the presence of an approximate C_2-symmetric structure. Additionally, the typical AB spin system of the bridging -CH_2- calixarene motif persists upon macrocycle formation, thus indicating that a cone conformation for **L** is maintained through self-assembly and through the structural reconfiguration sequence. As the most evident feature of the NMR spectra, the pyridyl protons Ha_{py} and Hb_{py} undergo significant broadening and downfield shifting upon binding to the Cu^{I} centres (Figure 2 and Supporting Information). Interestingly, the conversion of dinuclear $\mathbf{Cu_2L_2I_2}$ (**3**) into tetranuclear $\mathbf{Cu_4L_2I_4}$ (**4**) induced a slight downfield shifting of Ha_{py} protons; conversely, these Ha_{py} resonances experienced an upfield shifting upon transformation of dinuclear $\mathbf{Cu_2L_2Br_2}$ (**1**) into tetranuclear $\mathbf{Cu_4L_2Br_4}$ (**2**). Given that Cu_4X_4 are known to adopt diverse structural arrays, the difference in the NMR features of tetranuclear **2** and **4** (particularly the Ha_{py} resonances) suggests that these systems contain different types of Cu_4X_4 cores in their structures.

Diffusion-ordered NMR spectra (DOSY) showed that all resonances assigned to the macrocycles diffuse at the same rate (see Supporting Information); accordingly, the selective formation of a single species is confirmed, indicating that these macrocycles persist in solution as discrete and robust dinuclear or tetranuclear entities. The hydrodynamic radii (rH) of assemblies **1**–**4** nearly double the value determined for the free calixarene **L**, providing strong evidence for the larger dimensions of the metallic species and in reasonable concordance with the [2+2] $\mathbf{Cu^{I}_2L_2X_2}$ or [4+2] $\mathbf{Cu^{I}_4L_2X_4}$ formulations (Figure 2). Likewise, formation of higher-nuclearity oligomeric or mononuclear 1:1 CuLX species is also ruled out.

The molecular $\mathbf{Cu_nL_2X_n}$ (n = 2, 4) composition of **1**–**4** assemblies was confirmed by ESI-MS analysis (see Supporting Infor-

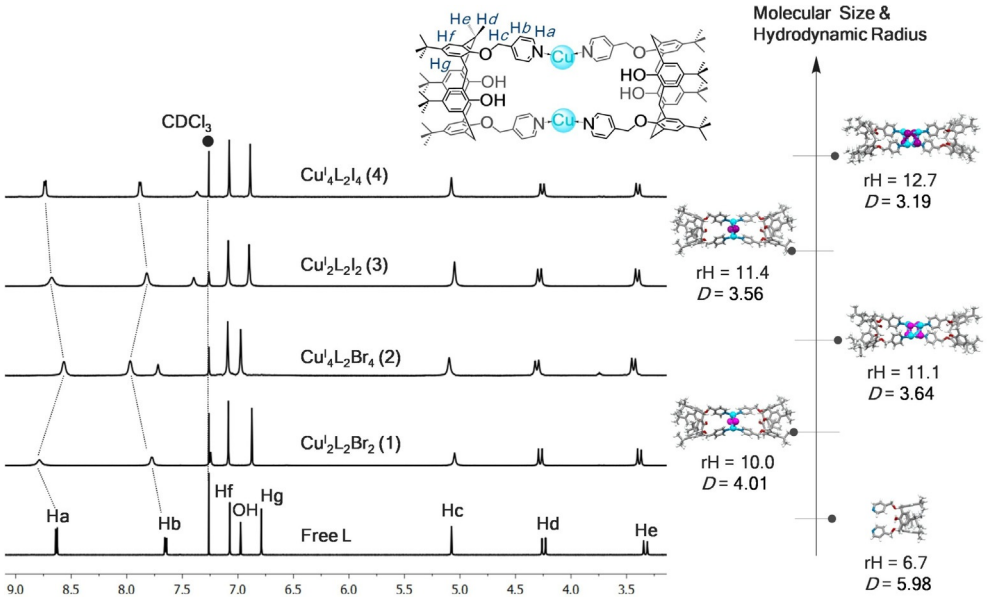

Figure 2. Partial ^{1}H NMR spectra of **L** and $\mathbf{Cu^{I}_{n}L_2X_n}$ metallacycles **1**–**4** in $CDCl_3$ at 25 °C, and graph showing measured diffusion coefficients (*D*) and calculated hydrodynamic radii (rH) for **L** and assemblies **1**–**4**.

mation). In all cases, the spectra are consistent with the formulation for the proposed macrocycles, as evidenced by the presence of $[\mathbf{Cu_nL_2X_{n-1}}]^+$ monocations as the most intense peaks arising from loss of one halogen anion; the experimental isotopic distributions are in good agreement with the calculated ones. It was also possible to observe charged states corresponding to species resulting from the capture of a free Cu^+ ion by the target di- or tetranuclear macrocycles; such reactivity under ESI-MS conditions is frequent for coordination supramolecules,[6] and their formation further witnesses to the presence of the proposed dinuclear or tetranuclear assemblies. As illustration of this, the spectrum of macrocycle $\mathbf{Cu_2L_2I_2}$ (**3**) shows intense peaks at 1915.7 *m/z* and 2105.5 *m/z*, assignable to $\{[\mathbf{Cu_2L_2I_2}]\text{-}I^-\}^+$ and $\{[\mathbf{Cu_2L_2I_2}]+Cu^+\}^+$ ions, respectively. Conversely, the ESI-MS spectrum of $\mathbf{Cu_4L_2I_4}$ (**4**) displays the same peaks as **3** along with signals corresponding to the larger $\{[\mathbf{Cu_4L_2I_4}]\text{-}I^-\}^+$ (*m/z* = 2297.4) and $\{[\mathbf{Cu_4L_2I_4}]+Cu^+\}^+$ (*m/z* = 2486.1) cations (Figure 3). Interestingly, peaks assignable to dinuclear fragments $[\mathbf{Cu_2L_2X}]^+$ were also detected in the spectra of tetranuclear complexes $\mathbf{Cu_4L_2Br_4}$ (**2**) and $\mathbf{Cu_4L_2I_4}$ (**4**) as transient species during disassembly (Figure 3). Accordingly, we infer that dinuclear macrocycles may be kinetic metastable intermediates during the construction of the tetranuclear architectures of **2** and **4**.

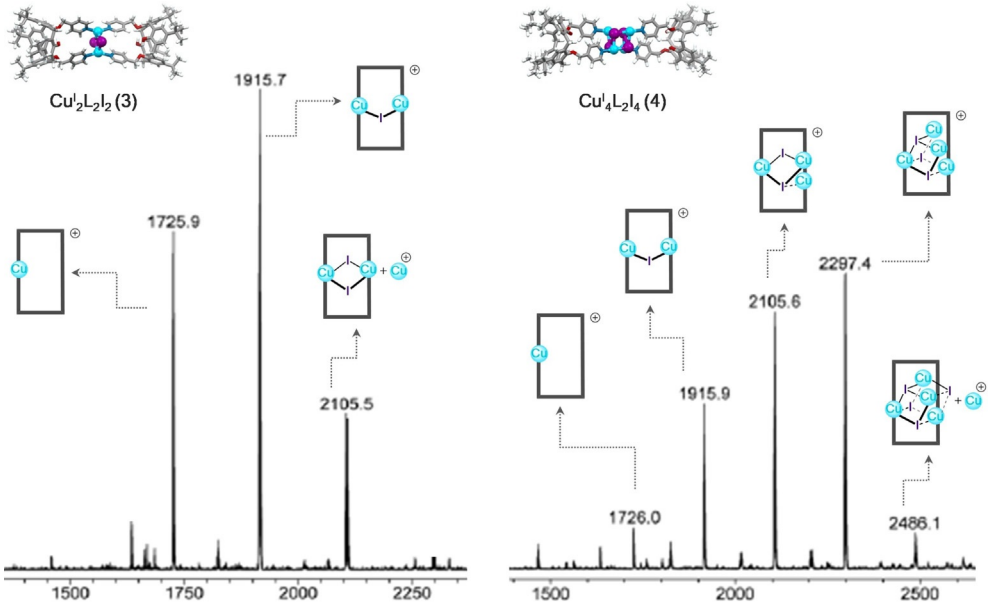

Figure 3. ESI-MS spectra of assemblies $\mathbf{Cu^{I}_2L_2I_2}$ (left) and $\mathbf{Cu^{I}_4L_2I_4}$ (right) in 4:1 CH_2Cl_2:CH_3CN evidencing their different nuclearity and common charged states.

Molecular mechanics (MM3) calculations predict that dinuclear complexes feature tetrahedral environments around Cu^{I} centres linked through bridging halogen ligands. It is also suggested that the tetranuclear macrocycles **2** and **4** might be assembled through Cu_4X_4 cubane-type clusters, which is the prevalent structural motif for emissive Cu_4X_4 coordination complexes among the available geometries for $[Cu_4X_4]$ clusters,[7] and it may account for the observed highly symmetric NMR pattern of these tetranuclear assemblies. Although we were not able to confirm the solid-sate structure of macrocycles **1**–**4** and the type of $[Cu_4X_4]$ clusters present in $\mathbf{Cu_4L_2Br_4}$ (**2**) and $\mathbf{Cu_4L_2I_4}$ (**4**), the solution characterisation by ^{1}H, DOSY NMR, and ESI-MS data, together with the emissive properties (*vide infra*) provide compelling evidence for the proposed structures of the coordination-assemblies.[6,8] The aforementioned techniques provide evidence of the differences among di- and tetranuclear entities, and confirm that they are persitent in solution.

The UV-vis spectra of **L** and macrocycles **1**–**4** in $CHCl_3$ exhibit a prominent absorption band at $\lambda_{max} = 280$ nm, assigned to π–π^* symmetry-allowed intraligand transitions; only minor absorbance variations are observed among the series. UV excitation of a $CHCl_3$ solution of free **L** ($\lambda_{ex} = 280$ nm; 17.0×10^{-6} M) produced modest blue emission; in contrast, assemblies **1**–**4** displayed intense red emission ($\lambda_{max} = 660$–670 nm, Figure 4a).

Notably, tetranuclear $\mathbf{Cu_4L_2I_4}$ (**4**) exhibited luminescence thermochromism. While a $CHCl_3$ solution of **4** displayed red luminescence at 298 K, a large hypsochromic shift to blue emission was observed upon freezing to 80 K ($\lambda_{max} = 667$ nm at 298 K to 464 nm at 80 K); the original red emission was recovered upon warming (Figure 4b). Similarly, **4** was not emissive as a solid at room temperature; nonetheless, it glowed with intense yellow colour under UV lamp irradiation after cooling to 80 K (Figure 4b). It has been widely described that this thermochromic behaviour results from the interplay of low and high-energy emissions. While the low-energy band originates from a triplet "cluster-centered" (^{3}CC) excited state combined with iodide-to-copper charge transfer and *d*-*s* transitions, the high-energy band is associated with a triplet halide-to-ligand charge transfer process (^{3}XLCT).[7e–f] The temperature-dependent predominance of one emission band over the other is ultimately related to the distortions in the Cu_4X_4 cluster and the Cu···Cu distances. Coupled to this, it is well known that Cu_4X_4 clusters may adopt diverse arrays such as step-, open- or closed-cubane forms.[7d,h] In this context, we may infer that the difference in the emission of **4** as a solid sample and in solution at low and room temperature could be due to the presence of structurally distinct Cu_4X_4-clusters within **4** in solid and solution forms. Such thermochromic qualities are well known for molecular CuI complexes that contain Cu_4I_4 cubane-clusters,[7] but they are unprecedented in the context of coordination-driven supramolecular complexes;[9] this observation further reinforces the notion of a Cu_4I_4 closed cubane cluster present within the structure of **4**.

We previously informed that the emission wavelength of analogous self-assembled $M_2L_2X_n$ macrocycles was independent on the d^{10}-metal identity ($M = Zn^{II}$, Pd^{II}, Ag^{I}, and Cd^{II}), rendering them blue emissive in all cases.[4] Remarkably, this initial investigation into the emissive properties of these complexes attests to the dramatic effect on wavelength emissions due to the incorporation of d^{10}-Cu^{I} into this synthetic platform.

Self-assembly of metallacycles $\mathbf{Cu^{II}_2L_2X_n}$ [X = Cl (5), OTf (7); *n* = 2, 4] and cage $\mathbf{[Cu^{II}_2L_4(\mu\text{-}Cl)]^{3+}}$ (6)

Calixarene **L** reacted with $CuCl_2$ in equimolar amounts in CH_3CN producing the non-emissive macrocycle $\mathbf{Cu^{II}_2L_2Cl_4}$ (**5**) as a green precipitate that was soluble in chlorinated solvents or mixtures of chlorinated solvents with CH_3CN and CH_3OH (Figure 1c); its non-emissive nature can be ascribed to the quencher nature of Cu^{II} ions. The ^{1}H NMR spectrum only displayed a set of broad signals, among which the ones corresponding to the picolyl groups are not identifiable due to their proximity to the paramagnetic Cu^{II} centres; conversely, Electron Spin Resonance (ESR) measurements confirmed the presence of cupric ions (isotropic $g = 2.12$). The ESI-MS spectrum showed intense peaks of singly-charged states for $\{[\mathbf{Cu^{II}_2L_2Cl_4}]\text{-}Cl^-\}^+$, $\{[\mathbf{Cu^{II}_2L_2Cl_4}]H^+\}^+$, and $\{[\mathbf{Cu^{II}_2L_2Cl_4}]\text{-}H^+ + Cu^{2+}\}^+$ species at $m/z = 1895.2$, 1931.8, and 1993.7, respectively, which support the dinuclear formulation for macrocycle **5** in solution; sequential loss of chloride anions was also observed (Figure S18). Slow evaporation of a 4:1 CH_3OH:CH_2Cl_2 solution of **5** afforded

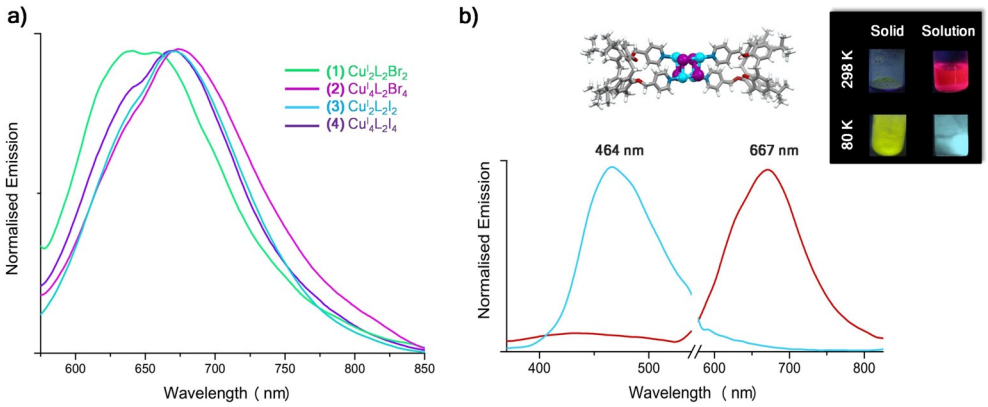

Figure 4. a) Emission spectra of metallacycles **1**–**4** (8.5×10^{-6} M; $\lambda_{ex} = 280$ nm) recorded in $CHCl_3$ at room temperature. b) Emission spectra measured at 80 K and 298 K evidencing luminescence thermochromism of **4**. Inset: photos of samples of **4** as solid and solution under UV light at 80 K and room temperature.

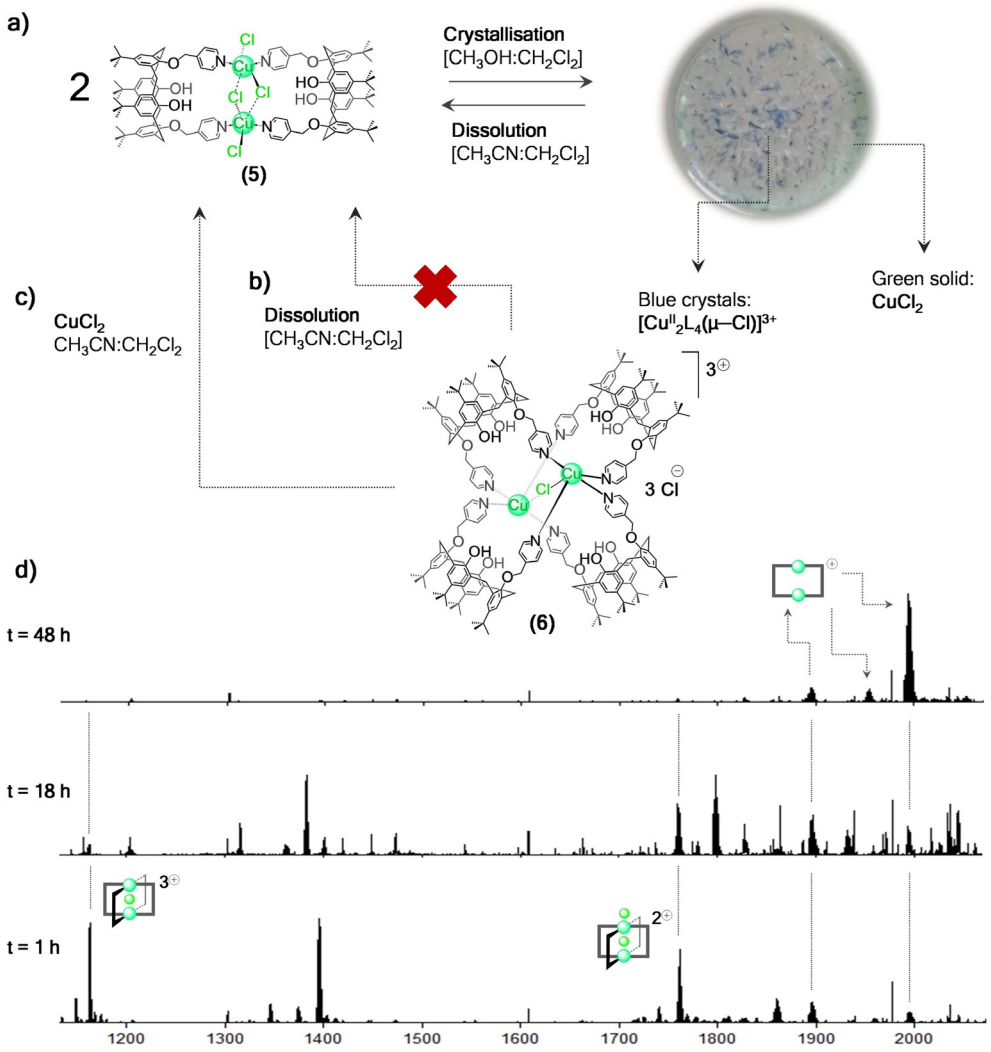

Figure 5. a) A mixture of crystals of cage **6** and $CuCl_2$ is obtained as response of **5** to CH_3OH (Inset: photo of the mixture); macrocycle **5** can be regenerated if the mixture is redissolved in presence of CH_3CN. b) Dissolution of crystals of cage **6** (no $CuCl_2$ added), does not yield macrocycle **5**; however, c) addition of $CuCl_2$ to a solution of cage **6** induces regeneration of **5**. d) HR-ESI mass spectrum of crystals of **6** mixed with $CuCl_2$ in CH_3CN:CH_2Cl_2, the doubly and triply charged states of cage **6** are highlighted.

blue crystals of a new complex (**6**) along with a green water-soluble solid identified as solvated $CuCl_2$ (Figure 5a). Although the metric parameters are not statistically ideal due to the very weakly diffracting nature of the crystals, the molecular structure and connectivity were firmly established. Unexpectedly, these blue crystals consisted of the cage **6** that differs from the composition determined for **5** in solution. Cage **$[Cu_2L_4(\mu\text{-}Cl)]^{3+}$** (**6**) displayed an overall windmill-like C_4-symmetric structure, in which four **L** units are arranged as the sails that are attached to a linear Cu-Cl-Cu axle (Figure 1d and Figure S31). In this array, the local coordination around Cu^{II} centres can be described as square pyramidal where four nitrogen atoms define the square plane and the linear chloride bridge of the axle bridges both cupric ions through the apical position. It was also possible to locate non-encapsulated chloride ions in the crystal packing that serve as linear connections between adjacent $[Cu_2L_4(\mu\text{-}Cl)]^{3+}$ units. Cage **6** was reversed to the parent macrocycle **5** only when crystals of **6** were dissolved in CH_3CN:CH_2Cl_2 and mixed with either the residual green solid that accompanies crystallisation or fresh $CuCl_2$ (Figures 1e and 5a).

ESI-MS studies were carried out on a solution (4:1 CH_3CN:CH_2Cl_2) containing blue crystals (cage **6**) mixed with the remaining green solid ($CuCl_2$); these measurements allowed further confirmation of the composition of cage **6**. Only within the first hour after dissolving the mixture, signals consistent with $[Cu_2L_4(\mu\text{-}Cl)]^{3+}$ ($m/z = 1162.28$) and $[Cu_2L_4(\mu\text{-}Cl)Cl]^{2+}$ ($m/z = 1760.90$) fragments of cage **6** were identified as the most intense peaks in the spectrum. Progressive emergence of ion peaks corresponding to macrocycle **5** (at $m/z = 1895.2$, 1931.8, and 1993.7) was observed over 48 h with concomitant disappearance of the peaks corresponding to **6** (Figures 5d and S21–S26). At intermediate time of conversion (spectrum measured after 18 h of mixing and dissolving), it was possible to distinguish peaks consistent with intermediate species mainly due to coordination of either CH_3OH or CH_3CN solvents (Figures 5d and S23). The overall process of crystallisation of **6** from a CH_3OH:CH_2Cl_2 solution of **5**, and conversion to **5** as response

of **6** to $CuCl_2$ stimulus can be carried out reversibly multiple times. Notably, we did not observe reconfiguration of cage **6** into of macrocycle **5** in absence of externally added $CuCl_2$ (Figure 5b), and all attempts to obtain cage **6** from direct synthesis by varying stoichiometry, concentration, and solvents were unsuccessful. Therefore, we may assume that cage **6** is a crystallisation product and a kinetic assembly that only dominates at high concentration and in the presence of the polar CH_3OH:CH_2Cl_2 solvent system. Conversely, macrocycle **5** is formed preferentially in dilute solution, and slow rearrangement of cage **6** into the thermodynamically stable metallacycle **5** takes place when suitable Cu^{II} signals are introduced (as $CuCl_2$) in the less polar CH_3CN:CH_2Cl_2 system (Figures 1e and 5c). It appears that both macrocycle **5** and cage **6** could be of similar energy and the formation of a given structure results from perturbations on a delicate balance between these two energetically similar structures; such solvent-responsive behaviour,[10] and disparity between solution and crystalline-state structures[11] has been observed in supramolecular coordination complexes.

Interestingly, when equimolar amounts of **L** and [Cu(MeCN)$_4$]OTf (OTf = $CF_3SO_3^-$) were mixed, macrocycle $\mathbf{Cu^{I}_2L_2(OTf)_2}$ (**7**) was obtained (Figure 1f). Colourless solutions of this complex in chlorinated solvents were readily oxidised as first evidenced by fast change in colour to blue-green. ESI-MS analysis of a CH_3CN:CH_2Cl_2 solution of **7** showed peaks consistent with the presence of oxidised Cu^{II} centres within the dinuclear cation $[\{Cu^{II}_2L_2(OTf)_2\}\text{-}H]^+$ (Figure S29). ^{1}H NMR studies in $CDCl_3$ revealed the presence of broad peaks indicative of an oxidised Cu^{II}-paramagnetic complex. Blue crystals were obtained from this NMR solution by slow evaporation, and despite their low-diffraction and loss of crystallinity, it was possible to unambiguously determine the molecular structure. Unexpectedly, the windmill-like cage $\mathbf{[Cu_2L_4(\mu\text{-}Cl)]^{3+}}$ (**6**) was found (Figure 1g). We inferred that **7** may abstract chlorine from chlorinated solvents; the oxidative abstraction of chlorine from organic compounds and solvents by Cu^{I} complexes is well documented.[12] It appears that the labile coordination of triflate anions renders complex **7** metastable and prone to be easily oxidised to cage **6**. Considering the ease of crystallisation of **6** and its apparent affinity for chloride, we prepared a $\mathbf{Cu^{II}_2L_2Br_4}$ metallacycle analogous to **5** just to test its potential to form a bromide analogue of **6** (see Supporting Information). No evidence of cage formation was found by ESI-MS (Figure S30), and all efforts to obtain crystals of macrocyclic or cage structures of the bromo compounds were unsuccessful. The latter observation further suggests that the central pocket in the $[Cu^{II}_2L_4]$ core of **6** discriminates bromide, and it is selective for the smaller chloride anion.

Conclusions

In summary, we have prepared a series of Cu-based supramolecular assemblies that express selective chemical and physical responses to external stimuli by virtue of the plasticity of N→Cu connections combined with the photoactive and redox properties of copper. In this manner, the control over nuclearity and functions has been exerted by addition of copper ions, allowing us to establish which structures may be observed under a certain set of conditions. Likewise, the luminescent properties of the supramolecular assemblies could be manipulated, from on and off, to tuning the emission wavelength. The structural and functional control by chemical signalling has been demonstrated with a set of related Cu-based supramolecules for the first time. Accordingly, our findings offer a singular platform to comprehend dynamic and adaptable systems, which is unprecedented for copper-based coordination-driven assemblies, particularly those with controllable luminescent architectures.

Experimental Section

Materials and methods

Reagents were purchased from commercial suppliers and used as received. All solvents were purified and distilled under N_2 by standard methods prior to use. Melting points were determined on an Electrothermal Mel-Temp apparatus and are uncorrected. Infrared spectra were obtained with a Bruker Tensor 27 spectrometer in the 4000–400 cm^{-1} spectral region as KBr disks. Electron Ionisation mass spectrometry (ESI MS) experiments were performed with a Bruker Daltonics Esquire 6000 spectrometer with ion trap; the diverse copper-assemblies were dissolved in a 1:4 MeCN:DCM mixture and filtered achieving concentrations in the range of 0.5–1.5 mM. EPR spectra were recorded at room temperature or at 77 K in quartz tubes with a JEOL JES-TE300 spectrometer operating at the X-band frequency (9.4 GHz) at 100 KHz field modulation with a cylindrical cavity (TE011 mode). NMR spectra were recorded with a Bruker Avance III 400 or with a Bruker 300 with tetramethylsilane (TMS) as an internal standard. The ^{1}H-DOSY spectra were recorded at 25 °C with 150 ms diffusion delay and 32 transients, using the 2D diffusion measurement Stimulated Echo & Led Bipolar Gradient (PFG-LED) with 2 spoil gradient ledgs2s pulse sequence in the standard Bruker pulse sequence library. Sample concentration of 10.0 mM was used to reduce viscosity changes and intermolecular interactions. Hydrodynamic radii in $CDCl_3$ were calculated by using the viscosity value $\eta CDCl_3 = 0.542\times10^{-3}$ kg m^{-1}·s^{-1}, 298 K. Absorption spectra were obtained as $CHCl_3$ solutions at 42.5×10^{-6} M concentration on an Agilent UV-vis spectrophotometer model 8453. All emission spectra were recorded on a Fluorolog Horiba Spectrofluorometer equipped with a Xe lamp; the samples (8.5×10^{-6} M) were excited at wavelength of absorption maxima $\lambda_{max} = 280$ nm, all emission measurements were carried out with 5 nm slit widths. Molecular modelling of macrocycles was performed using MM3 Energy-minimisation methods with the software package SCIGRESS 3.1.9.

Synthesis of compounds 1–7

All macrocycles were obtained through a similar protocol; preparation of macrocycle **1** is described below, while detailed synthetic procedures for the rest of copper-assemblies are provided in the Supporting Information.

$\mathbf{Cu^{I}_2L_2Br_2}$ (1). To a solution of copper (I) bromide (18.9 mg, 0.13 mmol) in acetonitrile was added **L** (100.2 mg, 0.12 mmol) in three portions under N_2 over 30 minutes. The resulting suspension was further stirred at room temperature for 14 h, and the precipitate obtained was vacuum filtered and washed with cold acetonitrile to give **1** as a pale gray solid. Yield: 196.5 mg, 85%; m.p.: 174–

175 °C (decomposition). IR (KBr): $\tilde{\nu}$ = 3364.6, 2958.9, 1612.0 cm^{-1} (C=N). ^{1}H NMR (400 MHz, $CDCl_3$, 25 °C): δ = 8.79 (br, 8H, Py), 7.78 (br, 8H, Py), 7.24 (s, 4H, OH), 7.09 (s, 8H, Ar), 6.87 (s, 8H, Ar), 5.05 (s, 8H, OCH_2-), 4.27 (d, $^2J_{H\text{-}H}$ = 13.0 Hz, 8H, -CH_2-), 3.38 (d, $^2J_{H\text{-}H}$ = 13.1 Hz, 8H, -CH_2-), 1.30 (s, 36H, *t*Bu), 0.98 ppm (s, 36H, *t*Bu). ^{13}C NMR (75 MHz, $CDCl_3$, 25 °C): δ = 150.8, 150.4, 149.1, 148.7, 148.0, 142.0, 132.6, 127.1, 125.9, 125.3, 122.4, 75.9, 34.1, 33.9, 31.7, 31.5, 31.0 ppm. DOSY Diffusion coefficient = $4.01 \pm 0.05 \times 10^{-10}$ $m^2 s^{-1}$. ESI-MS (+): *m/z* = 1868.7 $[Cu^{I}_2L_2Br]^+$, 1725.9 $[Cu^{I}L_2]^+$.

X-ray diffraction of cage 6

Blue crystals were obtained from slow evaporation of a MeOH/DCM solution of macrocycle **5**. All attempts to obtain high-quality data from X-ray diffraction experiments using these blue crystals (characterised as cage **6**) were unsuccessful due to their very weakly diffracting nature that might be related to the extensive presence of disordered anions, solvent molecules and crystalline voids. Moreover, some loss of crystallinity was observed upon solvent evaporation giving also rise to fractures. Crystals needed to be mounted at low temperature (130 K); however, it was only possible to observe weak diffractions using both molybdenum and copper radiations, seemingly due to a high volume of frozen solvent.

The general procedure was carried out as follows: a blue crystal was first cryoprotected using Paratone-N and mounted on a glass fiber; then, the crystal was immediately cooled at 130 K using Cryojet cryostream (Oxford Cryosystems device). Diffraction data were collected on an Oxford Diffraction Gemini diffractometer with a CCD-Atlas area detector using as radiation source, a graphite monochromator, $\lambda_{Cu\ K\alpha}$ = 1.54184 Å. CrysAlisPro and CrysAlis RED software packages were used for data collection and integration.[13] The Double Pass Method of scanning was used to exclude any noise and the collected frames were integrated by using an orientation matrix determined from the narrow frame scans. Final cell constants were determined by a global refinement; collected data were corrected for absorbance by using analytical numeric absorption correction using a multifaceted crystal model based on expressions upon the Laue symmetry using equivalent reflections.[14] Structure solution and refinement were carried using SHELXS-2014[15] and SHELXL-2014[16] software packages, and WinGX v2014.1 software was used to prepare material for publication.[17] Full-matrix least-squares refinement was carried out by minimising $(Fo^2\text{-}Fc^2)^2$. All non-hydrogen atoms were refined anisotropically. H atoms of water molecules were located in the difference map and refined isotropically with $U_{iso}(H) = 1.5$ for H-O. H atoms attached to C atoms were placed in geometrically idealised positions and refined as riding on their parent atoms, with C–H = 0.95–0.98 Å, and with $U_{iso}(H) = 1.2Ueq(C)$ for aromatic and methylene groups, and $U_{iso}(H) = 1.5Ueq(C)$ for methyl groups. Loss of crystallinity during data collection resulted in high R1 values and reduced quality data. Given that chloride anions and solvent molecules were significantly disordered, they could not be modelled properly; therefore, SQUEEZE from PLATON package of crystallographic software, was used to calculate the disordered areas and to remove their contributions to the overall intensity data.[18] The disordered solvent area is centred around the 0.00, 0.36, 0.00 position, and it shows an estimated total of 1267 electrons and a void volume of 4576 Å^3. Crystal data and experimental details of the structure determination of **6** are listed in Table S1. CCDC 1576400 contains the supplementary crystallographic data for this paper. These data can be obtained free of charge from The Cambridge Crystallographic Data Centre.

Acknowledgements

E.G. P. fully acknowledges DGAPA-UNAM for a postdoctoral fellowship. The authors thank Dr. M. Vonlanthen for assistance with emission measurements, V. Gómez-Vidales for ESR, L. Ríos and L. Márquez for ESI-MS.

Conflict of interest

The authors declare no conflict of interest.

Keywords: calixarenes · copper complexes · self-assembly · stimuli-responsiveness · supramolecular chemistry

[1] A. J. McConnell, C. S. Wood, P. P. Neelakandan, J. R. Nitschke, *Chem. Rev.* **2015**, *115*, 7729 – 7793.
[2] a) W. Wang, Y.-X. Wang, H.-B. Yang, *Chem. Soc. Rev.* **2016**, *45*, 2656 – 2693; b) L. Xu, Y.-X. Wang, L.-J. Chen, H.-B. Yang, *Chem. Soc. Rev.* **2015**, *44*, 2148 – 2167.
[3] Some selected examples: a) D. Samanta, P. S. Mukherjee, *Chem. Eur. J.* **2014**, *20*, 12483 – 12492; b) G. H. Clever, P. Punt, *Acc. Chem. Res.* **2017**, *50*, 2233 – 2243; c) Y. Fang, T. Murase, M. Fujita, *Chem. Asian J.* **2014**, *9*, 1321 – 1328; d) S. Wang, T. Sawada, K. Ohara, K. Yamaguchi, M. Fujita, *Angew. Chem. Int. Ed.* **2016**, *55*, 2063 – 2066; *Angew. Chem.* **2016**, *128*, 2103 – 2106; e) I. A. Riddell, M. M. J. Smulders, J. K. Clegg, Y. R. Hristova, B. Breiner, J. D. Thoburn, J. R. Nitschke, *Nat. Chem.* **2012**, *4*, 751 – 756; f) D. Preston, A. Fox-Charles, W. K. C. Lo, J. D. Crowley, *Chem. Commun.* **2015**, *51*, 9042 – 9045; g) I. A. Bhat, D. Samanta, P. S. Mukherjee, *J. Am. Chem. Soc.* **2015**, *137*, 9497 – 9502; h) E. G. Percástegui, J. Mosquera, J. R. Nitschke, *Angew. Chem. Int. Ed.* **2017**, *56*, 9136 – 9140; *Angew. Chem.* **2017**, *129*, 9264 – 9268; i) A. Sørensen, A. M. Castilla, T. K. Ronson, M. Pittelkow, J. R. Nitschke, *Angew. Chem. Int. Ed.* **2013**, *52*, 11273 – 11277; *Angew. Chem.* **2013**, *125*, 11483 – 11487.
[4] E. Guzmán-Percástegui, M. Vonlanthen, B. Quiroz-García, M. Flores-Alamo, E. Rivera, I. Castillo, *Dalton Trans.* **2015**, *44*, 15966 – 15975.
[5] a) V. W.-W. Yam, V. K.-M. Au, S. Y.-L. Leung, *Chem. Rev.* **2015**, *115*, 7589 – 7728; b) N. Armaroli, *Chem. Soc. Rev.* **2001**, *30*, 113 – 124; c) C. Lescop, *Acc. Chem. Res.* **2017**, *50*, 885 – 894; d) C. Fuertes-Espinosa, C. García-Simón, E. Castro, M. Costas, L. Echegoyen, X. Ribas, *Chem. Eur. J.* **2017**, *23*, 3553 – 3557; e) L. Gómez, A. Company, X. Fontrodona, X. Ribas, M. Costas, *Chem. Commun.* **2007**, 4410 – 4412; f) A. J. Boersma, B. de Bruin, B. L. Feringa, G. Roelfes, *Chem. Commun.* **2012**, *48*, 2394 – 2396; g) E. Guzmán-Percástegui, D. J. Hernández, I. Castillo, *Chem. Commun.* **2016**, *52*, 3111 – 3114; h) N. Le Poul, Y. Le Mest, I. Jabin, O. Reinaud, *Acc. Chem. Res.* **2015**, *48*, 2097 – 2105.
[6] Z. Qi, T. Heinrich, S. Moorthy, C. A. Schalley, *Chem. Soc. Rev.* **2015**, *44*, 515 – 531.
[7] a) A. Raghuvanshi, C. Strohmann, J.-B. Tissot, S. Clément, A. Mehdi, S. Richeter, L. Viau, M. Knorr, *Chem. Eur. J.* **2017**, *23*, 16479 – 16483; b) M. Vitalle, P. C. Ford, *Coord. Chem. Rev.* **2001**, *219*, 3 – 16; c) Q. Benito, X. F. Le Goff, S. Maron, A. Fargues, A. Garcia, C. Martineau, F. Taulelle, S. Kahlal, T. Gacoin, J.-P. Boilot, S. Perruchas, *J. Am. Chem. Soc.* **2014**, *136*, 11311 – 11320; d) M. Knorr, A. Bonnot, A. Lapprand, A. Khatyr, C. Strohmann, M. M. Kubicki, Y. Rousselin, P. D. Harvey, *Inorg. Chem.* **2015**, *54*, 4076 – 4093; e) Q. Benito, I. Maurin, T. Cheisson, G. Nocton, A. Fargues, A. Garcia, C. Martineau, T. Gacoin, J.-P. Boilot, S. Perruchas, *Chem. Eur. J.* **2015**, *21*, 5892 – 5897; f) E. Cariati, E. Lucenti, C. Botta, U. Giovanella, D. Marinotto, S. Righetto, *Coord. Chem. Rev.* **2016**, *306*, 566 – 614; g) K. Tsugea, Y. Chishina, H. Hashiguchi, Y. Sasaki, M. Kato, S. Ishizakac, N. Kitamura, *Coord. Chem. Rev.* **2016**, *306*, 636 – 651; h) A. Bonnot, M. Knorr, C. Strohmann, C. Golz, D. Fortin, P. D. Harvey, *J. Inorg. Organomet. Polym. Mater.* **2015**, *25*, 480 – 494.
[8] L. Avram, Y. Cohen, *Chem. Soc. Rev.* **2015**, *44*, 586 – 602.
[9] a) L. Xu, Y.-X. Wang, H.-B. Yang, *Dalton Trans.* **2015**, *44*, 867 – 890; b) B. Jiang, L.-J. Chen, Y. Zhang, H.-W. Tan, L. Xu, H.-B. Yang, *Chin. Chem. Lett.* **2016**, *27*, 607 – 612.

[10] a) Q. Chen, F. Jiang, D. Yuan, G. Lyu, L. Chen, M. Hong, *Chem. Sci.* **2014**, *5*, 483 – 488; b) J. Heo, Y.-M. Jeon, C. A. Mirkin, *J. Am. Chem. Soc.* **2007**, *129*, 7712 – 7713; c) B. Kilbas, S. Mirtschin, R. Scopellitia, K. Severin, *Chem. Sci.* **2012**, *3*, 701 – 704; d) K. Suzuki, M. Kawano, Makoto Fujita, *Angew. Chem. Int. Ed.* **2007**, *46*, 2819 – 2822; *Angew. Chem.* **2007**, *119*, 2877 – 2880; e) J.-J. Liu, Y.-J. Lin, Z.-H. Li, G.-X. Jin, *Dalton Trans.* **2016**, *45*, 13675 – 13679.
[11] a) A. Stephenson, S. P. Argent, T. Riis-Johannessen, I. S. Tidmarsh, M. D. Ward, *J. Am. Chem. Soc.* **2011**, *133*, 858 – 870; b) A. M. Najar, I. S. Tidmarsh, H. Adams, M. D. Ward, *Inorg. Chem.* **2009**, *48*, 11871 – 11881.
[12] a) B. Lucchese, K. J. Humphreys, D.-H. Lee, C. D. Incarvito, R. D. Sommer, A. L. Rheingold, K. D. Karlin, *Inorg. Chem.* **2004**, *43*, 5987 – 5998; b) D. Maiti, A. A. Narducci Sarjeant, S. Itoh, K. D. Karlin, *J. Am. Chem. Soc.* **2008**, *130*, 5644 – 5645.
[13] Agilent CrysAlis PRO and CrysAlis RED. Agilent Technologies, Yarnton, England, **2013**.
[14] R. C. Clark, J. S. Reid, *Acta Crystallogr. Sect. A* **1995**, *51*, 887 – 897.
[15] G. M. Sheldrick, *Acta Crystallogr. Sect. A* **2015**, *71*, 3 – 8.
[16] G. M. Sheldrick, *Acta Crystallogr. Sect. C* **2015**, *71*, 3 – 8.
[17] L. J. Farrugia, *J. Appl. Crystallogr.* **1999**, *32*, 837.
[18] a) A. L. Spek, *Acta Crystallogr. Sect. C* **2015**, *71*, 9 – 18; b) A. L. Spek, *Acta Crystallogr. Sect. D* **2009**, *65*, 148 – 155.

Manuscript received: December 14, 2017
Revised manuscript received: January 8, 2018
Accepted manuscript online: January 9, 2018
Version of record online: February 5, 2018